



# Trapped modes in a non-axisymmetric cylindrical waveguide

A.A. Lyapina, A.S. Pilipchuk, A.F. Sadreev<sup>\*</sup>

Kirensky Institute of Physics, Federal Research Center KSC SB RAS, 660036 Krasnoyarsk, Russia

## ARTICLE INFO

### Article history:

Received 4 February 2017

Revised 25 January 2018

Accepted 29 January 2018

Available online 8 February 2018

### Keywords:

Trapped modes

Cylindrical non-axisymmetric waveguide

Waveguide rotation

Wave faucet

## ABSTRACT

We consider acoustic wave transmission in a non-axisymmetric waveguide which consists of a cylindrical resonator and two cylindrical waveguides whose axes are shifted relatively to each other by an azimuthal angle  $\Delta\phi$ . Under variation of the resonator's length  $L$  and fixed  $\Delta\phi$  we find bound states in the continuum (trapped modes) due to full destructive interference of resonant modes leaking into the waveguides. Rotation of the waveguide adds complex phases to the coupling strengths of the resonator eigenmodes with the propagating modes of the waveguides tuning Fano resonances to give rise to a wave faucet. Under variation of  $\Delta\phi$  with fixed resonator's length we find symmetry protected trapped modes. For  $\Delta\phi \neq 0$  these trapped modes contribute to the scattering function supporting high vortical acoustic intensity spinning inside the resonator. The waveguide rotation brings an important feature to the scattering and provides an instrument for control of acoustic transmittance and wave trapping.

© 2018 Elsevier Ltd. All rights reserved.

## 1. Introduction

Bound states in the continuum are localized solutions which correspond to discrete eigenvalues coexisting with extended modes of continuous spectrum in resonator-waveguide configurations. The existence of such modes was first reported Neumann and Wigner [1] at the dawn of quantum mechanics. To the best of our knowledge, the term *bound state (embedded) in the continuum* was introduced by Fonda [2] in the context of resonance reactions in the presence continuous channels. Since then bound state in the continuum (BIC) has been universally used to designate a state with discrete energy embedded into the continuum in quantum mechanics [3]. In the field of fluid mechanics, Parker [4,5] is credited to be the first to encounter resonances of pure acoustic nature in air flow over a cascade of flat parallel plates. Nowadays, BICs are known to exist in various waveguide structures [6–9]. BICs are of immense interest, especially, in optics thanks to experimental opportunity to confine light in optical microcavities despite the fact that outgoing waves are allowed in the surrounding medium [10–15].

Independently considerable attention has been paid to BICs in perturbed acoustic waveguides. Many different geometrical configurations with Neumann boundary conditions have been studied. These studies have shown that the existence of trapped modes is very sensitive to choice of geometry. Up to now geometrical configurations have been chosen to reduce the effective dimension of the acoustic waveguide. Chronologically, the following specific perturbed acoustic waveguides were considered. In 1951 Ursell [16,17] considered a sphere placed on the axis of a cylindrical guide and showed that a trapped mode exists for a selected radius of the sphere. There is a long history of trapped modes bound below the channel cut-off in two- and three-dimensional nonuniform waveguides due to the curvature of the waveguide or a localized bulge [18–21]. However the bound states with isolated discrete eigenvalue embedded in the continuous spectrum above the channel cut-off, BICs, are more unusual. Evans and Porter first provided convincing numerical evidence for BICs of both Neumann and Dirichlet types in the case of a

<sup>\*</sup> Corresponding author.

E-mail address: [almas@tnp.krasn.ru](mailto:almas@tnp.krasn.ru) (A.F. Sadreev).

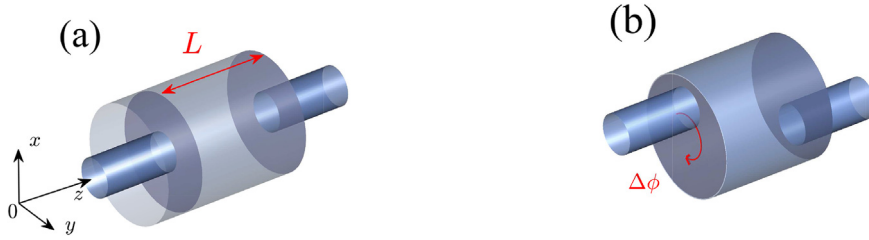


**Fig. 1.** Cylindrical resonator of radius  $R$  and length  $L$  with two attached cylindrical waveguides of the unit radius. All lengths are non-dimensional and measured in terms of the waveguide's radius  $r_w$ . The whole waveguide system is (a) axisymmetric, and (b) non-axisymmetric with waveguides misaligned by an azimuthal angle difference  $\Delta\phi$ .

rigid circular cylinder placed on the center-plane between parallel walls [22]. Linton and McIver [23] proved the existence of an infinite number of trapped modes for the case of a cylindrical waveguide containing an axisymmetric obstacle, in particular, a thin circular sleeve.

Similarly, the dimension is reduced in the acoustical waveguides of a rectangular cross-section in the  $yOz$  plane and directed along the  $x$ -axis with an obstacle shaped only in the  $xOy$  plane so that the thickness of the perturbed waveguide along the  $z$ -axis  $d$  is constant. Then the scattering channels are given by the eigenmodes quantized along the  $z$ -axis with corresponding Neumann boundary conditions at the walls positioned at  $z = \pm d/2$ . The utmost case of these structures is a two-dimensional acoustical waveguide formed by two infinite parallel lines at distance  $d$  containing a circle of radius  $R < d$  [24] or multiple circles [25,26] positioned symmetrically between them. The trapped modes are antisymmetric about the centerline of the guide, which allows us to determine them as symmetry protected BICs. More sophisticated BICs of the same symmetry as the symmetry of the continuum were demonstrated recently in Refs. [27–30].

A different class is the fully three-dimensional systems. For example, in the case of non-axisymmetric obstacle inside the cylindrical waveguide Hein and Coch [31] numerically computed acoustic resonances and BICs by solving the eigenvalue problem. Here we consider similar non-axisymmetric waveguide but without an obstacle inside as shown in Fig. 1. The axisymmetric case shown in Fig. 1 (a) preserves the orbital angular momentum (OAM)  $m$  because of the rotational symmetry around the central axis. That effectively reduces the dimension of the waveguide to two. The BICs with  $m = 0$  were shown to occur under variation of the length of the resonator [29] due to full destructive interference of resonant states [32]. An equivalent explanation of BICs is that under variation of the resonator length, the eigenmodes  $\psi_1, \psi_2$  of the same symmetry as the symmetry of propagating modes of the waveguides become degenerate. Then, the coupling of the superposed state  $a_1\psi_1 + a_2\psi_2$  with the continuum can be cancelled by a proper choice of the superposition coefficients  $a_1$  and  $a_2$  [33]. In the present paper, we choose a different strategy for the trapping of acoustic waves by means of the rotation of one of the waveguides by the angle  $\Delta\phi$  as shown in Fig. 1 (b). Then, one of the waveguides acquires azimuthal difference relative to the other that crucially affects interference of resonances, i.e., Fano resonances and the wave transmission. We show that even tiny rotations result in change of the transmittance from zero to unit, qualifying the setup as a wave faucet.

## 2. Acoustic coupled mode theory for open cylindrical resonators

There are different numerical approaches to calculate the transmittance through the waveguide with the mode matching method. The finite-element method with complex scaling is also widely exploited [28]. Here, we apply the method of effective non-Hermitian Hamiltonian [34–37] or, equivalently, the coupled mode theory, a physically transparent approach to diagnose BICs. The theory is based on the Feshbach projection technique [34] of the total space, resonator plus waveguides, onto the subspace of the resonator that results in the effective non-Hermitian Hamiltonian. Each subsystem possesses the rotational symmetry and obeys the stationary Helmholtz equation in the cylindrical system of coordinates

$$\left[ \frac{\partial^2}{\partial r^2} + \frac{1}{r} \frac{\partial}{\partial r} - \frac{m^2}{r^2} + \frac{\partial^2}{\partial z^2} + \omega^2 \right] \psi = 0, \quad (1)$$

for the non-dimensional velocity potential  $\psi$ , where the non-dimensional coordinates  $r$  and  $z$  express the respective distances normalized by the waveguide radius  $r_w$ . The dimensionless frequency  $\omega$  is defined through the dimensional frequency  $\tilde{\omega}$  as follows  $\omega = \tilde{\omega}r_w/c_0$ , and  $c_0$  is the sound speed [28].





The propagating modes in the sound hard cylindrical waveguides with Neumann boundary conditions are described by

$$\psi_{pq}(\rho, \alpha, z) = \psi_{pq}(\rho) \frac{1}{\sqrt{2\pi k_{pq}}} \exp(ip\alpha + ik_{pq}z), \quad (2)$$

$$\psi_{pq}(\rho) = \begin{cases} \frac{\sqrt{2}}{J_0(\mu_{0q})} J_0(\mu_{0q}\rho), & p = 0, \\ \sqrt{\frac{2}{\mu_{pq}^2 - p^2}} \frac{\mu_{pq}}{J_p(\mu_{pq})} J_p(\mu_{pq}\rho), & p = 1, 2, 3, \dots, \end{cases}$$

**Table 1**

Cut-off frequencies and corresponding shapes of propagating modes in the circular waveguide.

Channel	Cut-off frequency	Indices	Mode shape
1	0	$p = 0, q = 1$	
2	1.84118	$p = \pm 1, q = 1$	
3	3.0542	$p = \pm 2, q = 1$	
4	3.831706	$p = 0, q = 2$	

where  $\rho, \alpha$  are the polar coordinates in the  $xOy$ -plane, and  $\mu_{pq}$  is the  $q$ -th root of equation

$$\left. \frac{dJ_p(\mu_{pq}\rho)}{d\rho} \right|_{\rho=1} = 0$$

imposed by the Neumann boundary condition on the walls of sound hard cylindrical waveguide.

$$k_{pq}^2 = \omega^2 - \mu_{pq}^2 \quad (3)$$

The propagating bands degenerate with respect to the sign of OAM are classified by two indices: the OAM index  $p = 0, \pm 1, \pm 2, \dots$  and the radial index  $q = 1, 2, 3, \dots$ . The profiles of propagating functions  $\psi_{pq}(\rho) \cos(p\alpha)$  are depicted in Table 1.

The Hilbert space of the closed cylindrical resonator is given by the following eigenmodes

$$\Psi_{mnl}(r, \phi, z) = \psi_{mn}(r) \sqrt{\frac{1}{2\pi}} \exp(im\phi) \psi_l(z), \quad (4)$$

where

$$\psi_{mn}(r) = \begin{cases} \frac{\sqrt{2}}{R J_0(\mu_{0n}R)} J_0\left(\frac{\mu_{0n}r}{R}\right), & m = 0 \\ \sqrt{\frac{2}{\mu_{mn}^2 - m^2}} \frac{\mu_{mn}}{R J_m(\mu_{mn}R)} J_m\left(\frac{\mu_{mn}r}{R}\right), & m = 1, 2, 3, \dots, \end{cases} \quad (5)$$

$$\psi_l(z) = \sqrt{\frac{2 - \delta_{l,1}}{L}} \cos[\pi(l-1)z/L],$$

$l = 1, 2, 3, \dots$ . The corresponding eigenfrequencies are

$$\omega_{mnl}^2 = \left[ \frac{\mu_{mn}^2}{R^2} + \frac{\pi^2 (l-1)^2}{L^2} \right] \quad (6)$$

where  $\mu_{mn}$  is the  $n$ -th root of the equation  $\left. \frac{dJ_m(\mu_{mn}r)}{dr} \right|_{r=R} = 0$  which follows from the Neumann BC on the walls of a sound hard cylindrical resonator. Note that the non-dimensional radius  $R$  and length  $L$  of the resonator are measured in terms of the waveguide radius  $r_w$ .

Given the Hermitian Hamilton operator of the whole system as

$$\mathbf{H} = \mathbf{H}_B + \sum_{C=L,R} (\mathbf{H}_C + \mathbf{W}_{BC} + \mathbf{W}_{CB}), \quad (7)$$

the projection onto the discrete subspace of the eigenmodes (4) leads to the effective non-Hermitian Hamiltonian [34–36]

$$\mathbf{H}_{\text{eff}} = \mathbf{H}_B + \sum_{C=L,R} \mathbf{W}_{BC} \frac{1}{\omega^2 + i0 - \mathbf{H}_C} \mathbf{W}_{CB}. \quad (8)$$

Here  $\mathbf{H}_B$  is the Hamiltonian of the closed resonator;  $\mathbf{H}_C$  is the Hamiltonian of the waveguides, left and right, with the continual eigenvalue spectrum given by Eq. (3);  $\mathbf{W}_{BC}$ ,  $\mathbf{W}_{CB}$  stand for the coupling matrix elements between the eigenmodes (4) and the eigenmodes of the scattering channels (2) with the frequency  $\omega$ . The term  $\omega^2 + i0$  ensures that only outgoing waves will be present in the solution after the scattering occurs. As a result, the effective Hamiltonian (9) is a non-Hermitian matrix with complex eigenvalues  $z_\lambda$  which determine the positions and widths of the resonant states as  $\text{Re}(z_\lambda)$ , and  $-2\text{Im}(z_\lambda)$  correspondingly

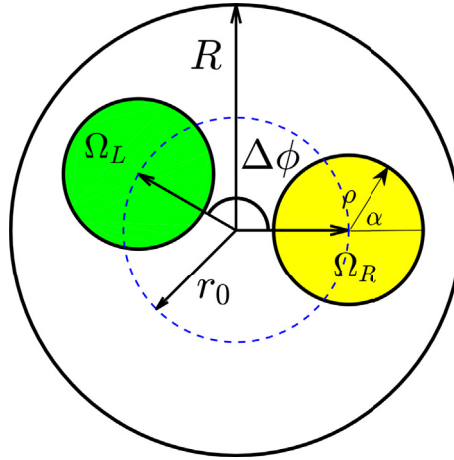


**Fig. 2.** Integration area in the coupling matrix (10) shown by filled areas.  $r_0$  is a distance by which the centerline of the waveguides are shifted relative to the centerline of the resonator.

[35,36]. Then, the Feshbach projection of the total space of the waveguide shown in Fig. 1 onto the subspace of the eigenmodes of the closed cylindrical resonator (4) gives us the following effective Hamiltonian [38]

$$\mathbf{H}_{\text{eff}} = \mathbf{H}_B - i \sum_{C=L,R} \sum_{pq} k_{pq} \mathbf{W}_{C,pq} \mathbf{W}_{C,pq}^\dagger \tag{9}$$

The full Hamiltonian (7) of an open system is Hermitian only in the total Hilbert space, which is spanned by the bound states and the scattering continuum states. The effective Hamiltonian (9), however, is non-Hermitian because of the leakage of the eigenmodes (4) into the open channels of the waveguides through the holes. That is why the eigenvalues of the non-Hermitian effective Hamiltonian are complex. The matrix elements of  $\mathbf{W}$  are given by overlapping integrals [38,39]

$$\begin{aligned} W_{mnl;pq}^C &= \int_{\Omega_C} \rho d\rho d\alpha \psi_{pq}(\rho, \alpha) \Psi_{mnl}^*(r, \phi, z = z_C) \\ &= \int_0^{2\pi} d\alpha \int_0^1 \rho d\rho \psi_{pq}(\rho, \alpha) \Psi_{mnl}^*(r(\rho, \alpha), \phi(\rho, \alpha), z_C) \\ &= \psi_l(z_C) \int_0^{2\pi} d\alpha \int_0^1 \rho d\rho \psi_{pq}(\rho, \alpha) \psi_{mn}^*(r(\rho, \alpha), \phi(\rho, \alpha)), \end{aligned} \tag{10}$$

where  $\Omega_{C=L,R}$  are interfaces positioned at  $z_C = 0, L$  where the waveguides are attached to the resonator as shown in Fig. 2. Integration is performed over the circular cross section of the attached waveguides as shown in Fig. 2. One can link the polar coordinates of the resonator with that of the immovable waveguide

$$r \sin \phi = \rho \sin \alpha, r \cos \phi = r_0 + \rho \cos \alpha$$

where  $r_0$  is the distance between the axes of the waveguide and the resonator. According to Eq. (4) we have

$$\psi_l(z = 0) = \sqrt{\frac{2 - \delta_{l,1}}{L}}, \psi_l(z = L) = \psi_l(0)(-1)^{l-1}. \tag{11}$$

Although the waveguides are identical they are attached to the resonator at different azimuthal angles as shown in Fig. 2 to give rise to an exact relation between the coupling matrix elements

$$W_{mnl;pq}^L = (-1)^{l-1} e^{i(p-m)\Delta\phi} W_{mnl;pq}^R \tag{12}$$

Here  $W_{mnl;pq}^R = W_{mnl;pq}^R$  are the coupling matrix elements of the resonator modes specified by integers  $m, n, l$  with  $p, q$  propagating modes of the left waveguide (see Fig. 1). Then the matrix of the effective Hamiltonian takes the following form

$$\langle mnl | \mathbf{H}_{\text{eff}} | m' n' l' \rangle = \omega_{mnl}^2 \delta_{mm'} \delta_{nn'} \delta_{ll'} - i \sum_{pq} k_{pq} [1 + (-1)^{l+l'} e^{i(m'-m)\Delta\phi}] W_{mnl;pq} W_{m' n' l'; pq}^* \tag{13}$$

The transmittance of sound waves in the  $p, q$  propagating channel through the resonator is given by the following equation [38]

$$T_{pq;pq} = 2ik_{pq} \sum_{mnl} \sum_{m' n' l'} W_{mnl;pq} e^{-in'\Delta\phi} G_{mnl:m' n' l'} W_{m' n' l'; pq}^* \tag{14}$$

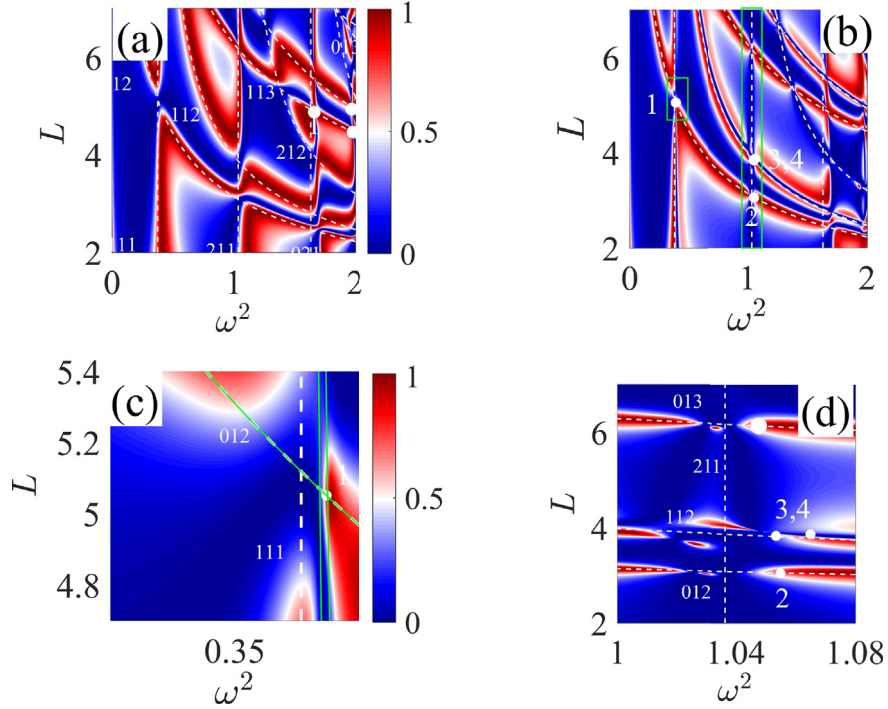


**Fig. 3.** Transmittance of a cylindrical resonator versus frequency squared and length of the resonator  $L$  at (a)  $\Delta\phi = 0$  and (b)  $\Delta\phi = \pi/4$ . (c) and (d) Zoomed transmittance in the domains isolated by rectangles in (b). Dash lines show eigenlevels of the closed resonator with corresponding indices  $mnl$ . Solid lines show eigenlevels of the resonator shifted by evanescent modes given by the modified Hamiltonian (18). The positions of the BICs are shown by closed circles.

where

$$\mathbf{G} = \frac{1}{\omega^2 - \mathbf{H}_{\text{eff}}}, \quad (15)$$

that is propagation of waves through the resonator is described by the Green function which is inverse of the matrix  $\omega^2 - \mathbf{H}_{\text{eff}}$  and coupling matrices of the resonator with the input (left) waveguide and the output (right) waveguide. However, the most remarkable feature in Eq. (14) is complex phases of the coupling matrix elements which contribute into interference of different states  $mnl$ . As we show below, that drastically affects Fano resonances.

### 3. Trapping under variation of the resonator length $L$

In what follows we take both waveguides with unit radius shifted relative to the central axis of the resonator with radius  $R = 3$  by a distance  $r_0 = 1.5$ . We consider transmission in the first channel  $p = 0, q = 1$  in the frequency region  $0 < \omega < 1.8412$  (see Table 1). The transmittance versus the frequency squared and the resonator length  $L$  is shown in Fig. 3 for  $\Delta\phi = 0$  and

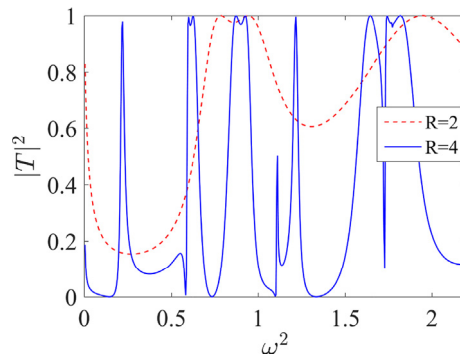


**Fig. 4.** The transmittance versus frequency squared for two values of the resonator's radius  $R$  at  $\Delta\phi = 0$ .

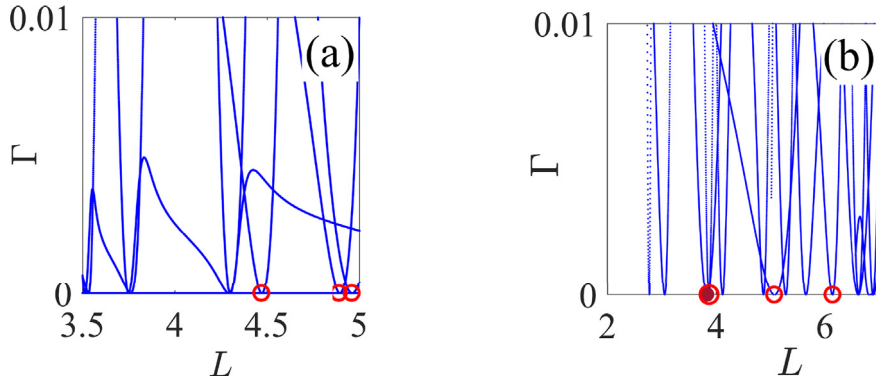


Fig. 5. Evolution of resonant widths under variation of the resonator length at  $\Delta\phi = 0$  (a) and  $\Delta\phi = \pi/4$  (b). Circles mark BICs listed in Tables 2 and 3.

Table 2

BICs at  $\Delta\phi = 0$ .

BIC	$\omega^2$	$L$	$mn\ell$	$a_{mn\ell}$
1	1.6617	4.8743	021	0.9276
			013	0.3665
2	1.9571	4.9371	$\pm 113$	0.6015
			$\pm 121$	0.5563
3	1.9795	4.465	013	-0.3228
			$\pm 311$	-0.1252

$\Delta\phi = \pi/4$ . Irrespective of the choice of the rotation angle, the transmittance has resonant behavior which is due to the fact that the resonator is three-dimensional. Indeed, the coupling matrix elements (10) can be estimated as the ratio of the cross section of the waveguides to the cross section of the resonator. The resonant widths are proportional to the coupling matrix elements squared, i.e., proportional to  $R^{-4}$  which follows from the normalization of the eigenmodes, while the distance between the eigenlevels  $\Delta E$  is proportional to  $R^{-2}$ . Hence, for a larger radius of the resonator we have the regime of weak coupling [40],

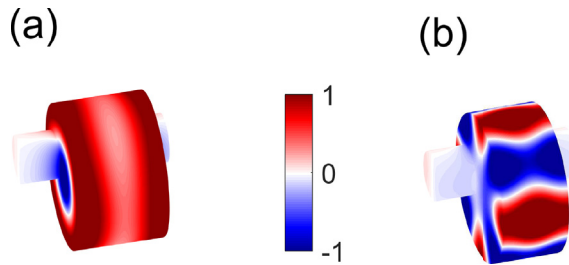


Fig. 6. Patterns of BIC 1 (a) and BIC 2 (b) from Table 2 on the surface of the waveguide at  $\Delta\phi = 0$ .

Table 3

BICs at  $\Delta\phi = \pi/4$ .

BIC	$\omega^2$	$L$	$mn\ell$	$a_{mn\ell}$	$ a_{mn\ell} $
1	0.385	5.065	012	$-0.113+0.272i$	0.294
			111	$-0.478(1-i)$	0.675
			-111	0.675	0.675
2	1.055	3.051	012	$-0.261(1-i)$	0.369
			211	0.656i	0.656
			-211	0.656	0.656
3	1.0535	3.833	211	0.658i	0.658
			-211	0.658	0.658
			112	$-0.237-0.098i$	0.256
4	1.065	3.869	-112	$-0.098-0.237i$	0.256
			211	-0.505	0.505
			-211	0.505	0.505
			112	$-0.455-0.189i$	0.493
			-112	$0.189+0.455i$	0.493

while for two-dimensional resonator one would have  $\Gamma \sim R^{-2}$  as well as  $\Delta E \sim R^{-2}$ , i.e., the regime of overlapping resonances [29]. This observation shows an important difference between planar and three-dimensional waveguides. Fig. 4 illustrates how the radius of the resonator affects the resonant transmission. In the two-dimensional systems the regime of weak coupling can be reached only by use of special diaphragms [41]. One of the advantages of the effective non-Hermitian Hamiltonian approach is that the BIC can be easily found as the eigenmode of the effective Hamiltonian

$$\mathbf{H}_{\text{eff}}\psi_r(r, \phi, z) = z_r\psi_r(r, \phi, z) \quad (16)$$

with zero resonant width, i.e., with real eigenvalue  $z_r$  [29,33]. Each BIC point is searched for by solving the fix point equations [35]

$$\omega_c = \text{Re}(z(\omega_c, L_c, \Delta\phi_c)), \quad \text{Im}(z(\omega_c, L_c, \Delta\phi_c)) = 0.$$

After the fix point equation is solved we can determine the eigenmodes of the effective Hamiltonian with real eigenvalues [29,33]. One can see from Eq. (14) that the above equation corresponds to the case when one of the poles of the S-matrix reaches real axis as was considered by Hein *et al* [31]. Then the Green function becomes singular. In order to avoid this singularity in the transmittance the coupling strength becomes zero. Rigorous consideration of these subtle features is given in Refs. [33,42].

### 3.1. Coaxial waveguides ( $\Delta\phi = 0$ )

Fig. 5 shows numerous events of the resonant widths turning to zero with variation of the resonator length  $L$  which evidence BICs. Inside the resonator the BIC trapped mode can be expanded over the eigenmodes of the closed resonator (4)

$$\psi_{\text{BIC}}(r, \phi, z) = \sum_{mnl} a_{mnl} \Psi_{mnl}(r, \phi, z). \quad (17)$$

The expansion coefficients of the BICs  $a_{mnl}$  are listed in Table 2, where we present only those BICs whose frequencies fit into the frequency window shown in Fig. 3 (a). They are marked by open circles in Fig. 5 (a). One can see from Table 2 that only a few eigenmodes of the resonator participate in the BIC expansion (17). The expansion coefficients are real and equal for  $\pm m$ . All BICs

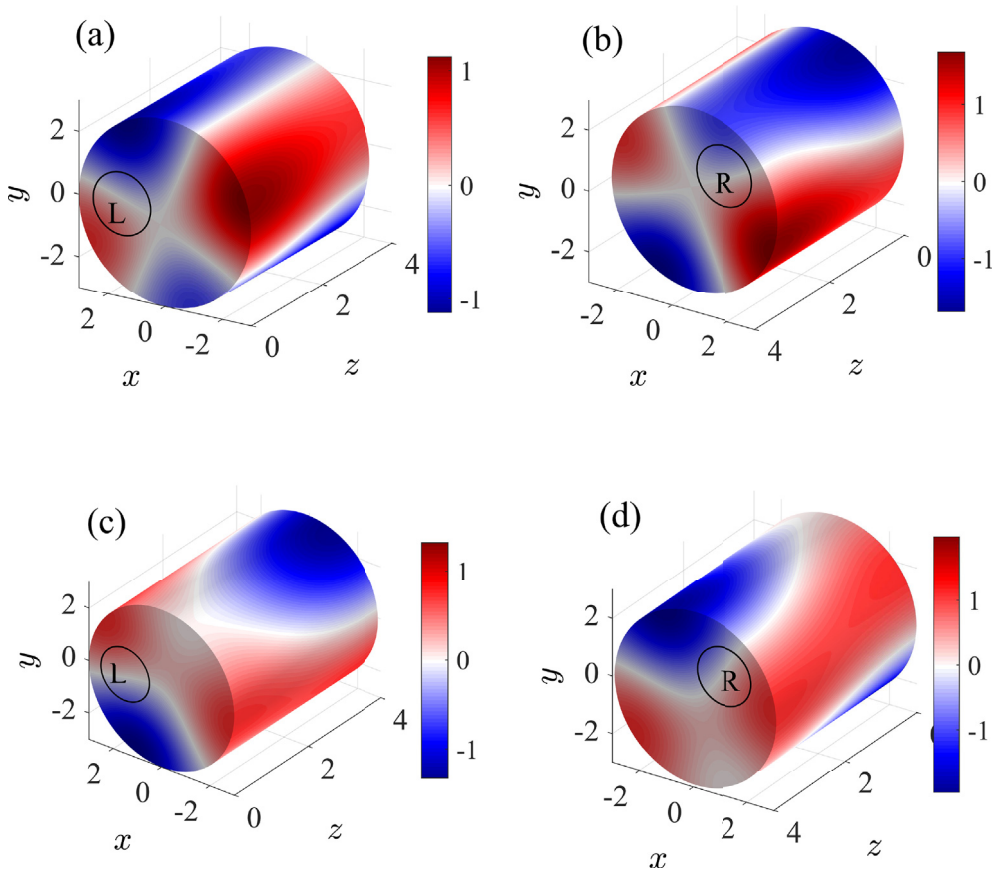
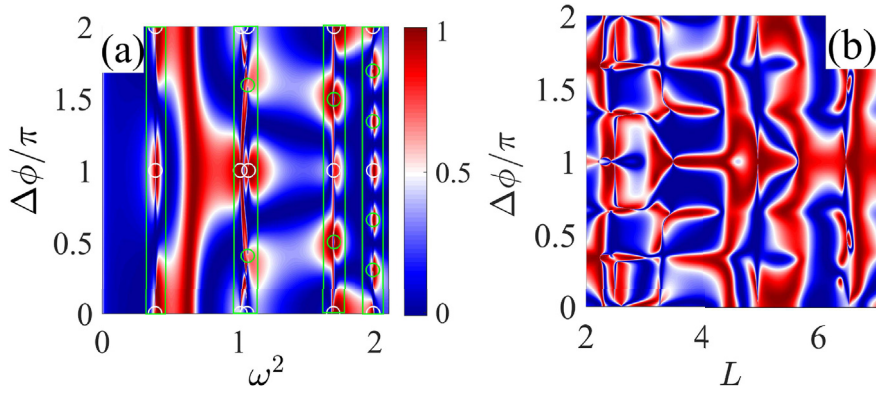
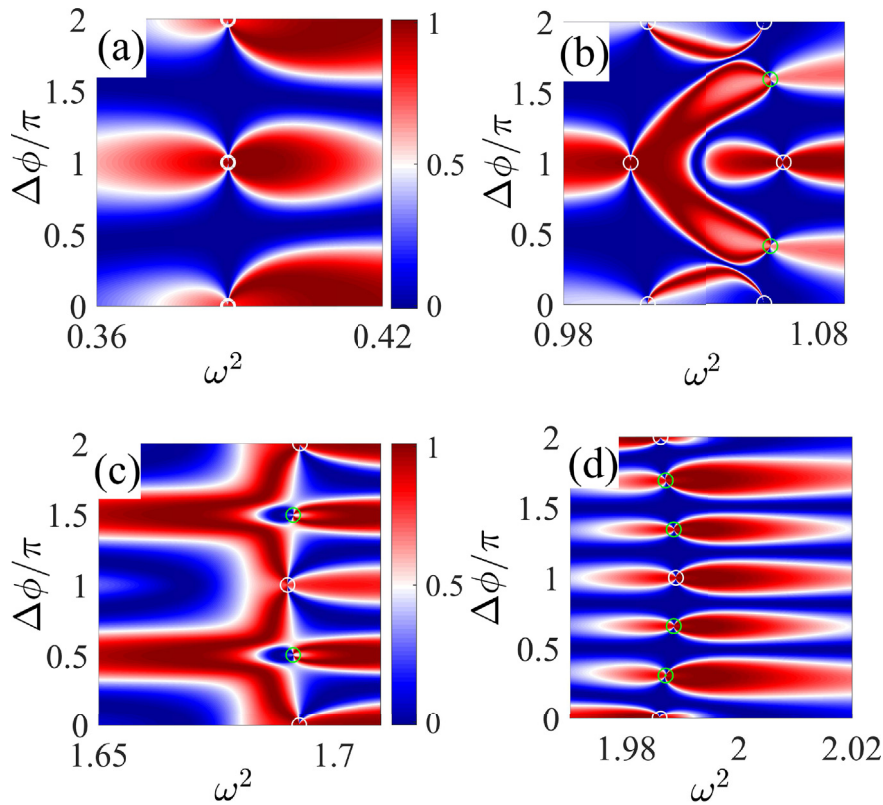


Fig. 7. Patterns of BIC 3 (a, b) and 4 (c, d) shown from the left (a, c) and right (b, d) sides of the resonator on the surface of the waveguide at  $\Delta\phi = \pi/4$ .



**Fig. 8.** Transmittance of a cylindrical resonator (a) versus frequency squared and rotation angle  $\Delta\phi$  at  $L = 4$  and (b) versus length and rotation angle at  $\omega^2 = 2$ . The positions of the BICs are shown by open circles.



**Fig. 9.** Transmittance versus frequency squared and rotation angle  $\Delta\phi$  at the resonator's length  $L = 4$  in frequency regions shown in Fig. 8 (a) by rectangles. The positions of the BICs are shown by closed circles. (a) The  $\omega^2$  region from 0.36 till 0.42, (b) the second from 0.98 till 1.08, (c) the third from 1.65 till 1.72, and (d) the fourth from 1.97 till 2.02.

listed in Table 2 are the result of the Friedrich-Wintgen mechanism of destructive interference [32,33] when the eigenmode  $m\ell n$  with the azimuthal part  $\cos(m\phi)$  crosses the eigenmode  $m'\ell'n'$  with the azimuthal part  $\cos(m'\phi)$ . In Fig. 6, we show BICs 1 and 2 listed in Table 2 on the surface of the waveguide similar to those shown by Hein *et al* [31]. We leave aside here the trivial symmetry protected BICs whose azimuthal dependence is given by  $\sin(m\phi)$ . It is clear that, for the waveguides with no phase difference these BICs have zero overlapping with the first channel  $p = 0, q = 1$  shown in Table 1.

### 3.2. Non-coaxial waveguides with $\Delta\phi = \pi/4$

In the preceding discussion we considered the BICs for the case when both waveguides were attached to the cylindrical resonator in a non-axisymmetric way for  $\Delta\phi = 0$ . That makes the effect of both waveguides identical, and summation over



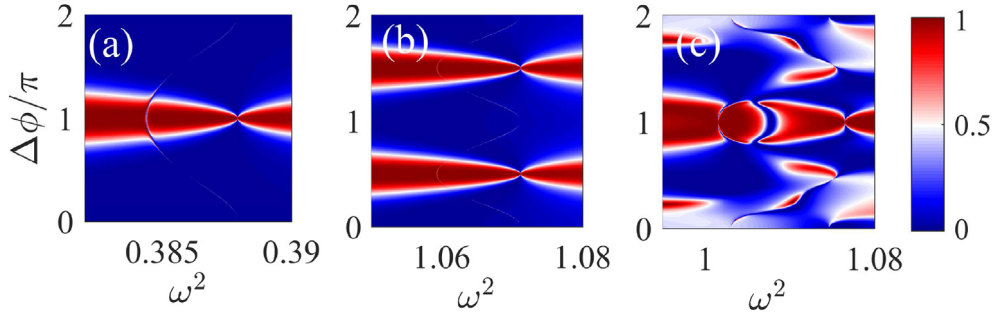


**Fig. 10.** Transmittance versus the frequency and rotation angle in the vicinity of crossing of the modes (a) 012 and  $\pm 111$  at  $L = 5$ , (b) 012 and  $\pm 211$  at  $L = 3$ , and (c)  $\pm 112$  and  $\pm 211$ ,  $L = 4$ .

$C = L, R$  in the effective Hamiltonian (9) simply gives rise to a factor of 2. Let us now shift the axis of the waveguides by an azimuthal angle  $\Delta\phi$  as shown in Fig. 1 (b). To be specific, we consider the case  $\Delta\phi = \pi/4$ . Although the continua of the waveguides remain the same, the rotation of the left waveguide provides the complex phases in the coupling matrix elements of the resonator eigenmodes with the continua as given by Eq. (12). This does not affect the transmittance except the points of crossing of the eigenlevels as shown in Fig. 3 (c) and (d).

As before the BIC points were detected by finding zero resonant width as shown in Fig. 5 (b). However, upon closer inspection in Fig. 3 (c) and (d), we see that these BICs are not exactly in the positions of the degeneracy of the eigenmodes of the closed resonator. The corresponding BICs are listed in Table 3 and shown in Fig. 7. Here we outline only the most important results. (i) The evanescent modes with imaginary  $k_{pq}$ ,  $p > 0$  contribute into the Hamiltonian of the closed resonator  $\mathbf{H}_R$  to modify it as follows

$$\tilde{\mathbf{H}}_B = \mathbf{H}_B + \sum_{C=L,R} \sum_{p>0,q} k_{pq} \mathbf{W}_{C,pq} \mathbf{W}_{C,pq}^+ \quad (18)$$

As a result, the BICs occur in the points of degeneracy of the eigenlevels of this Hamiltonian that explains the positions of the BICs shown in Fig. 3 (c).

(ii) If the waveguides were coaxial with the resonator, the eigenmodes of  $\tilde{\mathbf{H}}_B$  given by the azimuthal parts  $\cos(m\phi)$  and  $\sin(m\phi)$  (or equivalently,  $e^{im\phi}$  and  $e^{-im\phi}$ ) of the cylindrical resonator would be degenerate. However, as soon as the waveguides are attached non-coaxially, this degeneracy with respect to the sign of  $m$  is lifted as shown in Fig. 3 (c) by solid lines. This leads to the important consequence that the BICs of the non-coaxial waveguide cannot support currents of acoustic intensity [44] in contrast to the case of coaxial waveguides [27]. Fig. 7 clearly shows that BICs at  $\Delta\phi \neq 0$  are decoupled from the first channel. Assume that the BIC mode is decoupled from the right waveguide owing to degeneracy. In order for the BIC mode to be decoupled from the rotated left waveguide the BIC mode has to be twisted to compensate for this rotation [43,44]. Fig. 7 clearly illustrates the effect of twisting of the BIC by the rotation angle  $\Delta\phi$ .

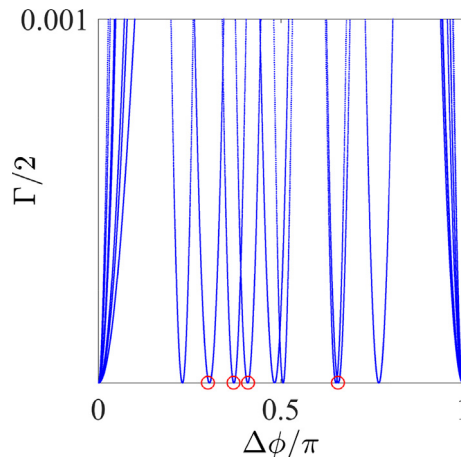


**Fig. 11.** Evolution of resonant widths under waveguide rotation at the resonator's length  $L = 4$ .

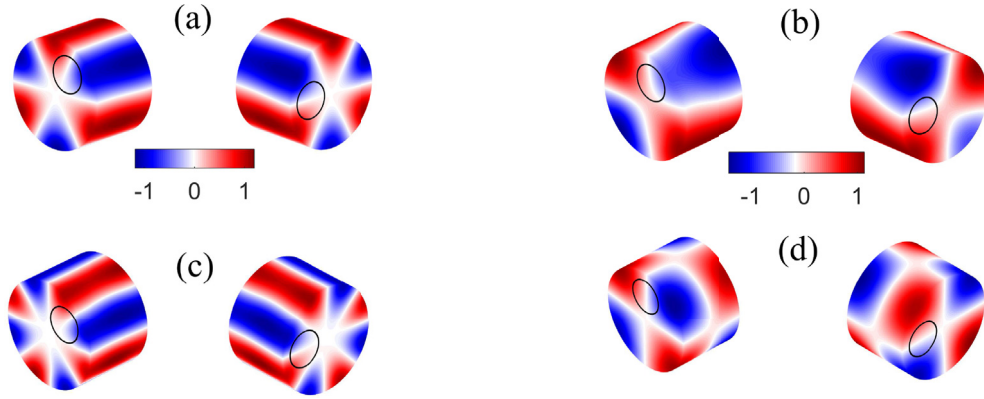


**Fig. 12.** Patterns of BICs marked by open circles in Fig. 11 and listed in Table 4 on the surface of the resonator at  $L = 4$ . (a) BIC 1, (b) BIC 3, (c) BIC 2, and (d) BIC 4. Open circles show where the left and right waveguides are attached to the resonator.

**Table 4**  
BICs at  $L = 4$ .

BIC	$\Delta\phi/\pi$	$\omega^2$	$ml$	$a_{mnl}$
1	0.308	1.9868	311	0.7056
			-311	$0.7056e^{-3i\Delta\phi}$
2	0.2351	3.17304	411	0.705
			-411	$0.705e^{4i\Delta\phi}$
3	0.4171	1.05688	211	0.6898
			-211	$-0.6898e^{-2i\Delta\phi}$
			121	$0.0933 + 0.1215i$
			-121	$a_{121}e^{i\Delta\phi}$
4	0.5055	1.68872	211	0.7043
			-211	$0.7043e^{-2i\Delta\phi}$

#### 4. Wave faucet

Eq. (14) shows that the phase factors in the coupling matrix elements due to the rotation of the input waveguide brings an important contribution into interference between resonances. Figs. 8 and 9 vividly illustrate high sensitivity of the transmittance to the rotation angle  $\Delta\phi$ . To clearly demonstrate this interference strongly affecting Fano resonances we present the transmittance in the vicinity of the crossing of eigenmodes in Fig. 10. As seen in Fig. 3 (a), the eigenmode 012 crosses the eigenmode  $\pm 111$  around  $L = 5$ . Correspondingly the transmittance is basically given by the interference of these resonances. According to Eq. (12) we have  $W_{012;01}^L = -W_{012;01}^R$ ,  $W_{\pm 111;01}^L = W_{\pm 111;01}^R e^{\mp i\Delta\phi}$ . Therefore for the output waves interfering constructively we have to take  $\Delta\phi = \pm\pi$ , while the full destructive interference takes place at  $\Delta\phi = 0$ . This simple consideration is in excellent agreement with numerics presented in Fig. 10 (a). Along the same line for channels 012 and  $\pm 211$  in the vicinity of  $L = 3$  we have from Eq. (12)  $W_{012;01}^L = -W_{012;01}^R$ ,  $W_{\pm 211;01}^L = W_{\pm 211;01}^R e^{\mp 2i\Delta\phi}$  to open wave flux through the resonator at  $\Delta\phi = \pi/2, 3\pi/2$ , which is illustrated in Fig. 10 (b). At last, in the vicinity of  $L = 4$  the eigenmodes  $\pm 112$  cross the eigenmodes  $\pm 211$ . Correspondingly we have  $W_{\pm 211;01}^L = W_{\pm 211;01}^R e^{\mp 2i\Delta\phi}$ ,  $W_{\pm 112;01}^L = -W_{\pm 112;01}^R e^{\mp 2i\Delta\phi}$  to give rise to constructive interference only at  $\Delta\phi = \pi$ , which agrees with Fig. 10 (c). Thus, the rotation of the input waveguide strongly tunes Fano resonance [43]. In particular there can be points in the transmittance where the maximum of transmittance approaches the transmission zeros. At these points, a collapse of Fano resonance occurs that signifies the existence of bound states in the continuum. These events are shown by open circles in Figs. 8 and 9 and confirmed by the behavior of the resonant widths versus the rotation angle as shown in Fig. 11. Among them we select four BICs shown in Fig. 12.

For  $\Delta\phi \neq 0$ , and arbitrary  $L$  the BICs are symmetry protected except in the case of a degeneracy of the resonator eigenmodes shown in Fig. 3. Indeed, let us consider the first BIC from Table 4 whose azimuthal dependence is given by  $\cos[3(\phi - \Delta\phi/2)]$ . In order to decouple this BIC from the right waveguide at  $\Delta\phi = 0$ , the nodal line of the BIC mode has to be positioned at  $\phi = 0$ , which gives us the equation  $\frac{3}{2}\Delta\phi = \frac{\pi}{2}$ , i.e.,  $\Delta\phi = \frac{\pi}{3}$ . Therefore the BIC mode is  $\cos[3(\phi - \pi/6)]$  which equals zero at  $\phi = 0$ . The left waveguide is rotated by the angle  $\pi/3$  for which the BIC mode is decoupled from the left waveguide too. Numerically according to Table 4 we have  $\Delta\phi = 0.308\pi$  which is close to  $\pi/3$ . The small difference is due to the evanescent modes. Similarly, for the second BIC we obtain  $\cos[4(\phi - \Delta\phi/2)]$ , which gives us  $\Delta\phi = \pi/4$  which is close to the numerical result  $\Delta\phi = 0.235\pi$  given in Table 4. For the fourth BIC we obtain that  $\Delta\phi = \pi/2$  which agrees well with Table 4. The most interesting is the third BIC which is superposed of two modes  $\cos[2(\phi - \Delta\phi/2)]$  and  $\cos[(\phi + \Delta\phi/2)]$ . As a result, the BIC mode is twisted as shown in Fig. 12.

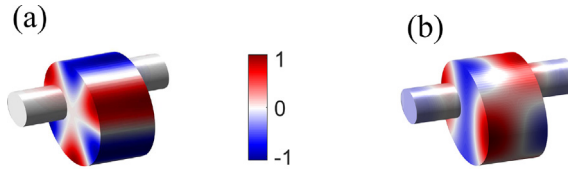


Fig. 13. Real parts of scattering function for the parameters close to the BIC point 4 given in Table 4. (a)  $\omega = \omega_c$  and (b)  $\omega = \omega_c + 0.01$ .

Although all of the BICs cannot support the flows of acoustic intensity, the scattering wave function calculated through the equation [37,38]

$$\begin{aligned} \psi(r', \phi', z) &= \frac{1}{\sqrt{4\pi k_{01}}} [e^{ik_{01}z} \phi_{10} + \sum_{pq} S_{01L;pqL} e^{-ik_{pq}z} \phi_{pq}(r', \phi')], \quad z < 0, \\ \psi_{mnl}(r, \phi, z) &= -i \sum_{m'n'l'} G_{mnl;m'n'l'} \sqrt{\frac{k_p}{\pi}} W_{m'n'l';01}^L, \quad 0 < z < L, \\ \psi_R(r', \phi', z) &= \frac{1}{\sqrt{4\pi k_{01}}} \sum_{pq} S_{01L;pqR} e^{ik_{pq}z} \phi_{pq}(r', \phi') z > L. \end{aligned} \tag{19}$$

is a complex superposition of the BIC and a particular solution of the scattering problem [33]. An example of the scattering function in the vicinity of BIC 4 in Table 4 is shown in Fig. 13. One can see that a small deviation from the BIC frequency results in a large change in the scattering function. This phenomenon constitutes the important effect of enhancement of the injected wave within the resonator [33,45,46].

What is even more interesting is that the scattering function supports vortical acoustic intensity as demonstrated in Fig. 14. The non-dimensional mean intensity vector  $\mathbf{j}$  follows  $-\nabla \arg(\psi)$  and is given by Refs. [47–49]

$$\mathbf{j} = -\omega \text{Im}(\psi^* \nabla \psi) = -\omega |\psi|^2 \nabla \arg(\psi), \tag{20}$$

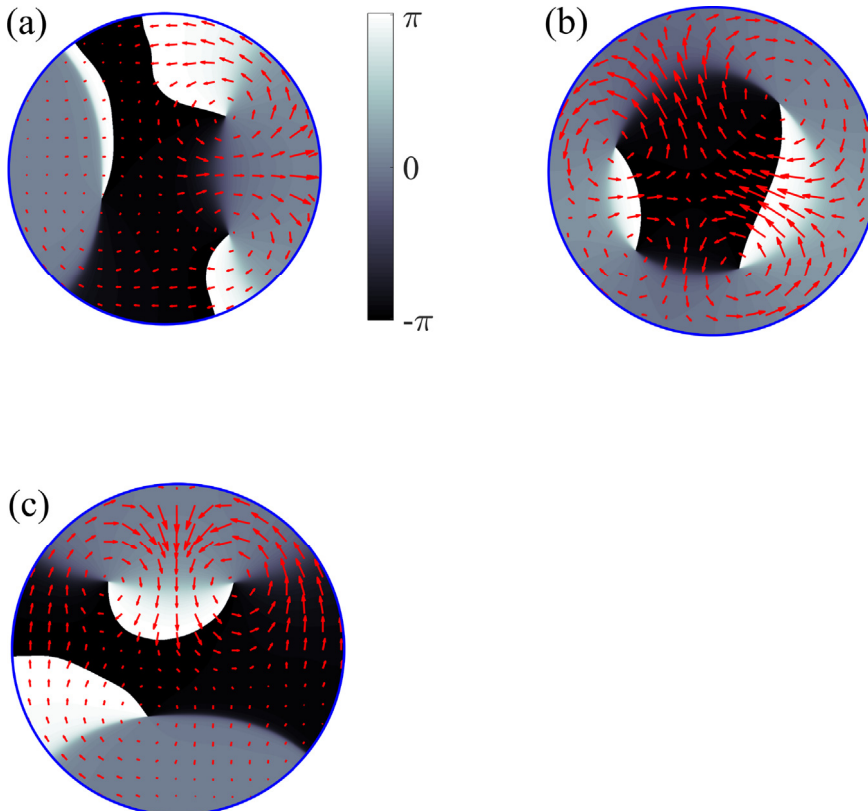


Fig. 14. Acoustic energy flow at different slices at the vicinity of the BIC 4: (a)  $z = 0$ , (b)  $z = L/2$ , and (c)  $z = L$ . The phase of the scattering function is shown in gray.

where  $\omega$  is the non-dimensional frequency defined after Eq. (1). The phase of the scattering function  $\arg(\psi)/\pi$  is shown in Fig. 14 for selected slices across  $z$ . Fig. 13 shows the scattering function (19) that demonstrates the effect of a twisted acoustic pressure field given by the real part of  $\psi$ . This figure is complemented with plots of the acoustic energy flow (20) in Fig. 14 which shows the complex vortical behavior of the acoustic intensity.

## 5. Conclusions

We considered trapped modes or bound states in the continuum in a non-axisymmetric duct-cavity structure which consists of a cylindrical resonator and two cylindrical waveguides whose axes are shifted relative to the axis of the resonator by a distance  $r_0$ . Moreover the axes of the waveguides can be shifted relative to each other by an azimuthal angle  $\Delta\phi$  as shown in Figs. 1 (b) and 2. The configuration of attachment does not change the eigenfrequencies of the closed resonator but changes the coupling strengths of the propagating modes of attached waveguides with the resonator. Remarkably, that rotation of, say, the input waveguide provides complex phases in the coupling strength that drastically affect the wave transmission because of interference of resonances giving rise to the effect of wave faucet. The effect can be arranged in a realistic acoustic experiment by the use of piston-like hollow-stem waveguides tightly fit to the interior boundaries of a cylindrical cavity [29].

Assume that the eigenmodes of the same symmetry undergo degeneracy, say, under variation of the resonator length  $L$  as shown by dash lines in Fig. 3. After the waveguides are attached to the resonator these modes become resonances which undergo avoided crossings, i.e., the resonant frequencies are repelled from each other and the degeneracy is lifted. Then, in the Friedrich-Wintgen scenario [32,33] one of the resonances can acquire zero resonant width giving rise to the BIC. Although the events of degeneracy are the same as in the closed cylindrical resonator, the types of BICs cardinal depend on the way of opening the resonator. For  $r_0 = 0$  (the case of axisymmetric waveguide) the OAM  $m$  is an integral of motion to give rise to the BICs with definite OAM degenerate with respect to the sign of  $m$ . Sound transmission takes place independently in each sector given by the  $m$ , i.e., there is no mode conversion between different the channels with different OAM. That scenario of BICs and sound transmission in axisymmetric cylindrical waveguide was considered in our first paper [29]. Similar sectorial BICs with preserved OAM were considered in Refs. [28,30,31].

As soon as  $r_0 \neq 0$ , even in the simplest case  $\Delta\phi = 0$  the OAM is not preserved because of the absence of rotational symmetry. In such cases we found multiple BICs with nonzero OAM under variation of the resonator length  $L$  which differ from the BICs with zero OAM found in the axisymmetric cylindrical waveguide [29]. Irrespective of the choice of  $r_0$ , the BICs occur at the points of degeneracy of two eigenmodes of the same symmetry of the closed cylindrical resonator. This mechanism of wave localization was first described in Ref. [32] and has been experimentally realized in microwave set-ups [50,51].

For  $\Delta\phi \neq 0$  and fixed arbitrary length of the resonator, there are multiple symmetry protected BICs whose azimuthal dependence is given by  $\cos[m(\phi - \Delta\phi/2)]$ . They are degenerate relative to the sign of  $m$  and provide zero overlapping with propagating mode  $p = 0, q = 1$  (see Table 1) which is independent of  $\phi$ . Irrespective of the choice of  $\Delta\phi$  or  $r_0$ , the injected wave with zero orbital angular momentum  $m = 0$  transmits and reflects with the same OAM when only the first channel is opened for the frequency  $\omega < 1.841$ . However, the case of  $\Delta\phi \neq 0$  is of special interest because of the twisted flows of the acoustic intensity inside the resonator. In this case the non-axial attachment of the waveguides with the resonator lifts the degeneracy of the resonant modes with respect to the sign of orbital angular momentum. These effects can be controlled by simultaneous variation of the length of the resonator and rotation of one of the waveguides. This results in a high acoustic intensity spinning inside the resonator which can be important for the axial radiation torque [52].

Summing up, the rotation of waveguide with respect to the cylindrical resonator results in a complex phase of the coupling strength between the waveguide and the resonator. Different setups can be proposed for the coupling strengths to acquire a specific phase difference. However, irrespective of the choice of the setup the opportunity to vary the phase opens a new possibility to control Fano resonances and the transmittance creating a wave faucet.

## Acknowledgement

This work has been supported by RFBR through Grant 17-02-00440. A.S. acknowledges discussions with E.N. Bulgakov, D.N. Maksimov, H. Schanz, P. Seba, L. Sirko, H.-J. Stöckmann and Shubo Wang.

## References

- [1] J. von Neumann, E.P. Wigner, Über merkwürdige diskrete eigenwerte (About strange discrete eigenvalue), *Z. Physik* 50 (1929) 291–293.
- [2] L. Fonda, Resonance reactions and continuous channels, *Ann. Phys.* 12 (1961) 476–484.
- [3] F. Stillinger, D. Herrick, Bound states in the continuum, *Phys. Rev.* 11 (1975) 446–454.
- [4] R. Parker, Resonance effects in wake shedding from parallel plates: some experimental observations, *J. Sound Vib.* 4 (1966) 62–72.
- [5] R. Parker, Resonance effects in wake shedding from parallel plates: calculation of resonant frequencies, *J. Sound Vib.* 5 (1967) 330–343.
- [6] J.U. Nöckel, Resonances in quantum-dot transport, *Phys. Rev. B* 46 (1992) 15348–15356.
- [7] C.S. Kim, A.M. Satanin, Y.S. Joe, R.M. Cosby, Resonant tunneling in a quantum waveguide: effect of a finite-size attractive impurity, *Phys. Rev. B* 60 (1999) 10962–10970.
- [8] O. Olendski, L. Mikhailovska, Bound state evolution in curved waveguides and quantum wires, *Phys. Rev. B* 66 (2002) 035331.
- [9] I. Rotter, A.F. Sadreev, Zeros in single-channel transmission through double quantum dots, *Phys. Rev. E* 71 (2005) 046204.
- [10] S. Shipman, S. Venakides, Resonant transmission near non robust periodic slab modes, *Phys. Rev.* 71 (2005) 026611.
- [11] D. Marinica, A. Borisov, S. Shabanov, Bound states in the continuum in photonics, *Phys. Rev. Lett.* 100 (2008) 183902.
- [12] E. Bulgakov, A. Sadreev, Bound states in the continuum in photonic waveguides inspired by defects, *Phys. Rev. B* 78 (2008) 075105.

- [13] Y. Plotnik, O. Peleg, F. Dreisow, M. Heinrich, S. Nolte, A. Szameit, M. Segev, Experimental observation of optical bound states in the continuum, *Phys. Rev. Lett.* 107 (2011) 183901.
- [14] Chia Wei Hsu, Bo Zhen, A.D. Stone, J.D. Joannopoulos, M. Soljačić, Bound states in the continuum, *Nat. Rev. Mater.* 1 (2016) 16048–16061.
- [15] A. Kodigala, T. Lepetit, Q. Gu, B. Bahari, Y. Fainman, B. Kanté, Lasing action from photonic bound states in continuum, *Nature* 541 (2017) 196–199.
- [16] F. Ursell, Trapping modes in the theory of surface waves, *Math. Proc. Camb. Phil. Soc.* 47 (1951) 347–358.
- [17] F. Ursell, Trapped modes in a circular cylindrical acoustic waveguide, *Proc. Roy. Soc. Lond. A* 435 (1991) 575–589.
- [18] P. Exner, P. Šeba, P. Štoviček, On existence of a bound state in L-shaped waveguide, *Czech J. Phys. B* 39 (1989) 1181–1191.
- [19] J. Goldstone, R.L. Jaffe, Bound states in twisting tubes, *Phys. Rev. B* 45 (1992) 14100–14107.
- [20] D. Duclos, P. Exner, Curvature-induced bound states in quantum waveguides in two and three dimensions, *Rev. Math. Phys.* 7 (1995) 73–102.
- [21] S.N. Gaultier, N.R.T. Biggs, Acoustic trapped modes in a three-dimensional waveguide of slowly varying cross section, *Proc. Royal Soc. A* 469 (2017) 1–17.
- [22] D.V. Evans, R. Porter, Trapped modes embedded in the continuous spectrum, *Q. Jl Mech. Appl. Math.* 52 (1998) 263–274.
- [23] C.M. Linton, P. McIver, Trapped modes in cylindrical waveguides, *Jl Mech. Appl. Math.* 51 (1998) 389–412.
- [24] M. Callan, C.M. Linton, D.V. Evans, Trapped modes in two-dimensional waveguides, *J. Fluid Mech.* 229 (1991) 51–64.
- [25] D.V. Evans, R. Porter, Trapped modes about multiple cylinders in a channel, *J. Fluid Mech.* 339 (1997) 331–356.
- [26] T. Utsunomiya, R.E. Taylor, Trapped modes around a row of circular cylinders in a channel, *J. Fluid Mech.* 386 (1999) 259–279.
- [27] Y. Duan, M. McIver, Rotational acoustic resonances in cylindrical waveguides, *Wave Motion* 39 (2004) 261–274.
- [28] S. Hein, W. Koch, L. Nannen, Trapped modes and Fano resonances in two-dimensional acoustical duct-cavity systems, *J. Fluid Mech.* 692 (2012) 257–287.
- [29] A.A. Lyapina, D.N. Maksimov, A.S. Pilipchuk, A.F. Sadreev, Bound states in the continuum in open acoustic resonators, *J. Fluid Mech.* 780 (2015) 370–387.
- [30] L. Xiong, W. Bi, Y. Aurégan, Fano resonance scatterings in waveguides with impedance boundary conditions, *J. Acoust. Soc. Am.* 139 (2016) 764–772.
- [31] S. Hein, W. Koch, Acoustic resonances and trapped modes in pipes and tunnels, *J. Fluid Mech.* 605 (2008) 401–428.
- [32] H. Friedrich, D. Wintgen, Interfering resonances and bound states in the continuum, *Phys. Rev. A* 32 (1985) 3231–3242.
- [33] A.F. Sadreev, E.N. Bulgakov, I. Rotter, Bound states in the continuum in open quantum billiards with a variable shape, *Phys. Rev. B* 73 (2006) 235342.
- [34] H. Feshbach, Unified theory of nuclear reactions, *Ann. Phys.* 19 (1962) 287–313.
- [35] J. Okołowicz, M. Płoszajczak, I. Rotter, Dynamics of quantum systems embedded in a continuum, *Phys. Rep.* 374 (2003) 271–383.
- [36] F.M. Dittes, The decay of quantum systems with a small number of open channels, *Phys. Rep.* 339 (2000) 215–316.
- [37] A.F. Sadreev, I. Rotter, S-matrix theory for transmission through billiards in tight-binding approach, *J. Phys. Math. Gen.* 36 (2003) 11413–11433.
- [38] D.N. Maksimov, A.F. Sadreev, A.A. Lyapina, A.S. Pilipchuk, Coupled mode theory for acoustic resonators, *Wave Motion* 56 (2015) 52–79.
- [39] K. Pichugin, H. Schanz, P. Seba, Effective coupling for open billiards, *Phys. Rev. E* 64 (2001) 056227.
- [40] V.V. Sokolov, V.G. Zelevinsky, Dynamics and statistics of unstable quantum states, *Nucl. Phys.* 504 (1989) 562–588.
- [41] S. Rotter, F. Libisch, J. Burgörfer, U. Kuhl, H.-J. Stöckmann, Tunable Fano resonances in transport through microwave billiards, *Phys. Rev. E* 69 (2004) 046208.
- [42] E.N. Bulgakov, I. Rotter, A.F. Sadreev, Comment on “Bound-state eigenenergy outside and inside the continuum for unstable multilevel systems”, *Phys. Rev. A* 75 (2007) 067401.
- [43] A.F. Sadreev, A.S. Pilipchuk, A.A. Lyapina, Tuning of Fano resonances by rotation of continuum: wave faucet, *Euro phys. Lett.* 117 (2017) 50011.
- [44] A.F. Sadreev, A.S. Pilipchuk, and A.A. Lyapina, Tuning of bound states in the continuum by waveguide rotation, arXiv: 1707.00864v1 [physics.app-ph].
- [45] Mingda Zhang, Xiangdong Zhang, Ultrasensitive optical absorption in graphene based on bound states in the continuum, *Sci. Rep.* 5 (8266) (2015) 1–7.
- [46] Maowen Song, Honglin Yu, Changtao Wang, Na Yao, Mingbo Pu, Jun Luo, Zuojun Zhang, Xiangang Luo, Sharp, Fano resonance induced by a single layer of nanorods with perturbed periodicity, *Optic Express* 23 (2015) 2895–2903.
- [47] R.V. Waterhouse, D. Feit, Equal-energy streamlines, *J. Acoust. Soc. Am.* 80 (1986) 681–684.
- [48] D.M.F. Chapman, Using stream lines to visualized acoustic energy flow across boundaries, *J. Acoust. Soc. Am.* 124 (2008) 48–56.
- [49] R.E. Musafir, On non-radiating sources, *J. Sound Vib.* 332 (2013) 3947–3955.
- [50] T. Lepetit, E. Akmansoy, J.-P. Ganne, J.-M. Lourtioz, Resonance continuum coupling in high-permittivity dielectric metamaterials, *Phys. Rev. B* 82 (2010) 195307.
- [51] T. Lepetit, B. Kante, Controlling multipolar radiation with symmetries for electromagnetic bound states in the continuum, *Phys. Rev. B* 90 (2014) 241103(R).
- [52] L. Zhang, P.L. Marston, Angular momentum flux of nonparaxial acoustic vortex beams and torques on axisymmetric objects, *Phys. Rev. E* 84 (2011) 065601(R).